Semi-circular potential sweep voltammetry: Experimental verification and determination of the formal potential of a reversible redox couple

Hatem M.A. Amin, Yuki Uchida, Enno Kätelhön and Richard G. Compton*

* Corresponding author: Richard G. Compton

Department of Chemistry, Physical & Theoretical Chemistry Laboratory, University of Oxford, South Parks Road, Oxford, OX1 3QZ, United Kingdom

Email: richard.compton@chem.ox.ac.uk, Tel: +44(0)1865275 957, Fax: +44(0)1865275410

Abstract

The use and merits of a semi-circular potential waveform in place of the conventional triangular waveform has been reported [J. Electroanal. Chem. 2018, 818, 140-148] on the basis of computational simulations. We report the experimental application of this new method to the study of the electrochemically reversible $[Ru(NH_3)_6]^{3+/2+}$ redox couple at a macroelectrode. The method is used to determine the formal potential of this redox couple. Agreement between theory and experiment is good.

Keywords: Cyclic voltammetry; Semi-circular waveform; Non-triangular waveform; Reversible reaction; Hexaminеruthenium(III) chloride; Linear sweep votammetry

1. Introduction

Cyclic voltammetry (CV) and linear sweep voltammetry (LSV) are the most widely used electrochemical techniques to gain important information on the kinetics, the mechanistics and the thermodynamics of many electrochemical reactions [1-4]. Analysis of the resulting voltammograms can yield useful data such as formal potentials, rate constants and transfer coefficients [5-9]. In addition, more recent techniques such as AC voltammetry [10, 11], ultrafast voltammetry [12-15] and pulse voltammetry [16-18] have been widely used for the analysis of redox species.

In CV, a triangular potential waveform is employed and the scan rate is hence constant throughout the entire potential window. The use of an alternative semi-circular potential waveform has been recently proposed based on simulations of semi-circular voltammograms for an electrochemical reversible process at macro- and micro-electrodes [19, 20]. The semi-circular wave generates an instantaneous nominally infinite scan rate at the midpoint of the applied potential window which significantly amplifies the current response at this potential, while slower scan rate are applied during other parts of the potential window which in turn reduce the current response. Voltammetric data can be used to determine the formal potential of a species and has been shown to be particularly useful if the formal potential of the species of interest is close to that of another interfering substance in solution or at low concentrations.

Here, we present an experimental validation of the theoretical analysis using the reversible Ru^{3+}/Ru^{2+} system. Experiments were conducted for the reduction of hexaammineruthenium(III) chloride, $[Ru(NH_3)_6]Cl_3$, at high aqueous electrolyte support levels at a glassy carbon macroelectrode. Voltammograms and peak currents show excellent agreement with theoretical results and are used for the determination of the formal potential of the redox species.

2. Semi-circular potential wave sweep voltammetry

This section gives a brief summary of the method employed. A detailed description can be found in our previous report [19].

In linear sweep voltammetry, the potential of the working electrode *E(t)* is swept linearly with respect to a reference electrode at a constant scan rate:

$$E(t) = E(t = 0) \pm \upsilon t \qquad (1)$$

where *E(t= 0)* is the initial potential and υ is the scan rate. An alternative approach with a semi-circular potential wave has recently been introduced by Uchida et al. [19, 20] and is rewritten as follows:

$$E(t) = \pm A_o \sqrt{|1 - \left[2\left(\frac{t}{t_{max}} - c\right)\right]^2|} + E_{centre} \qquad (2)$$

where A_o is the amplitude of the potential wave, t is the time and t_{max} is the duration of a single scan between the two potential limits. c = 0 for $t \leq t_{max}/2$ and c = 1 for $t_{max}/2 < t < t_{max}$.

For both sweeps, we define E_{centre} as the midpoint potential of the applied potential window relative to the reference electrode:

$$E_{centre} = \frac{E_f - E_i}{2} \qquad (3)$$

where E_i is the start potential and E_f is the final potential.

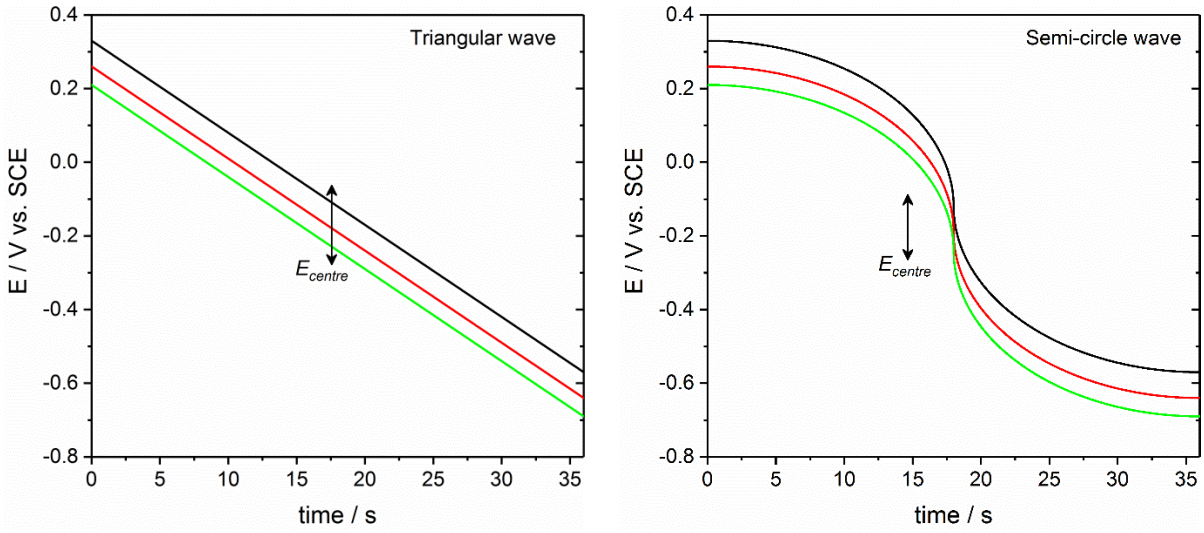

Fig. 1. Linear and semi-circular waveforms recorded for different E_{centre} values with an amplitude of 0.45 V.

The linear and semi-circular potential waveforms employed in this work for different potential windows are displayed in Fig. 1. For both potential waves, the duration of the scan is kept constant such that the average scan rate over the single potential scan is the same for semi-circular and linear waves. The triangular potential wave features a constant scan rate, while the semi-circular wave results in significant variations in the scan rate over the entire scan. At t = 0 and $t = t_{max}$, a scan rate close to zero is seen, whilst at E_{centre} the scan rate instantaneously approaches an infinite value. In contrast to CV studies where typically series of voltammograms are recorded for different scan rates, the potential E_{centre} at which this temporary fastest scan rate is reached is varied in semi-circle voltammetry.

3. Experimental

Hexaammineruthenium(III) chloride ($[Ru(NH_3)_6]Cl_3$,"Ruhex", Aldrich, 98%) and potassium chloride (KCl, Aldrich, >99%) were used as received. All solutions were prepared with Milli-Q water with a resistivity of 18.2 MΩ cm^{-1} at 298 K (Millipore Water Systems, UK). Prior to each experiment all solutions were bubbled for at least 30 min with N_2 (99.998%, BOC, U.K.) and then were blanketed with N_2 during the entire measurement. Experiments were conducted in a solution of 0.265 mM Ruhex in 0.50 M KCl and also in 1.0 mM Ruhex / 0.10 M KCl solution for comparison.

All electrochemical experiments (CV and LSV) were conducted using an in-lab built potentiostat, similar to the previously described one [21]. A three-electrode one-compartment glass cell was used, with a glassy carbon disc (GC, 3.08 mm diameter, ALS Co. Ltd, Japan) as the working electrode, a saturated calomel electrode (SCE, ALS Co. Ltd, Japan) as the reference electrode and a Pt wire (GoodFellow, Cambridge, U.K.) as the counter electrode. The GC electrode was polished before experiments with MicroPolish alumina (1, 0.3 and 0.05 μm from Buehler, IL, USA, one minute for each size in a descending order) onto soft lapping pads (Buehler, U.S.A.), followed by ultra-sonication in acetone and then in Milli-Q water (for 1 min in each) and finally dried under nitrogen flow. Before sweeping the potential within the desired potential window, the working electrode was held at the start potential (E_i) for 3 s.

A low noise potentiostat was used to control the potential of the working electrode discretised in intervals of nominally 60 μV. A USB-6003 DAQs (National Instruments, TX) was used for digital-to-analog and analog-to-digital conversions. To measure the current at the working electrode, a low current-amplifier DLPCA-200 (Femto Messtechnik GmbH, Berlin, Germany) was used and the bandwidth of the output of the current amplifier was limited using two cascaded 2 kHz passive RC-filters. The resulting analog signal was sampled at a stream rate of 100 kHz. *Python* Software was used to collect the data, while OriginPro 2017 was used for plotting.

All experiments were performed at 298 K and the temperature was kept constant using a water bath connected to a temperature controller (SCT1, Stuart, U.K.) inside a Faraday cage.

4. Results and Discussion

In this section we first address the differences in the voltammetry that result from linear and semi-circular potential waves. Second we analyse voltammograms recorded for a series of shifted potential windows. Third we investigate the voltammetric behaviour at different voltage scan rates and fourth we determine the formal potential of the Ru^{3+}/Ru^{2+} redox couple.

Throughout the entire work, we investigate the reversible one-electron reduction of $[Ru(NH_3)_6]^{3+}$ to $[Ru(NH_3)_6]^{2+}$ at a planar macrodisc glassy carbon electrode in an aqueous electrolyte under diffusion-only conditions [22-24] as a model system, where a high electrolytic support is used to supress migration [22], and both species are assumed to have equal diffusion coefficients:

$$Ru^{3+} + e^{-} \rightleftharpoons Ru^{2+} \quad (4)$$

All simulations are performed using a *finite difference* code previously described [19].

4.1. Voltammetry with triangular and semi-circular potential waveforms

We first discuss the effect of the triangular wave versus the recently proposed semi-circular potential wave on the voltammetric behaviour of the electrochemically reversible $[Ru(NH_3)_6]^{3+/2+}$ system. Fig. 2 shows the voltammograms obtained using both linear and semi-circular potential waveforms for the potential range of 0.23 V to −0.67 V (E_{centre}= −0.22 V) at an average scan rate of 0.025 V s^{-1} in both blank solution of 0.5 M KCl and in 0.265 mM $[Ru(NH_3)_6]Cl_3$/0.5 M KCl solution. In linear sweep voltammetry, a peak for the reduction of Ru^{3+} appears at −0.23 V, see Fig. 2a. In blank 0.5 M KCl solution (blue graphs), the triangular voltammetry does not show a typical half rectangle in the capacitive currents but a slight current increase at potentials more negative to −0.3 V which is possibly due to residual oxygen in solution. On the contrary, the capacitive currents obtained using the semi-circular voltammetry are variable with a sharp peak at the midpoint of the applied potential window. This is due to the occurrence of the fastest scan rate in the immediate vicinity of this potential value. Since, for a constant interface capacitance, the capacitive current is directly proportional to scan rate, a large increase in capacitive current is observed at this potential while relatively low currents are seen everywhere else.

In all voltammograms, unless otherwise stated, to plot the faradaic-only currents (red graphs), the capacitive currents obtained in blank 0.5 M KCl solution are subtracted from the measured currents in $[Ru(NH_3)_6]Cl_3$/KCl solution (green graphs) and the voltammograms are base-line corrected, as shown in Fig. 2.

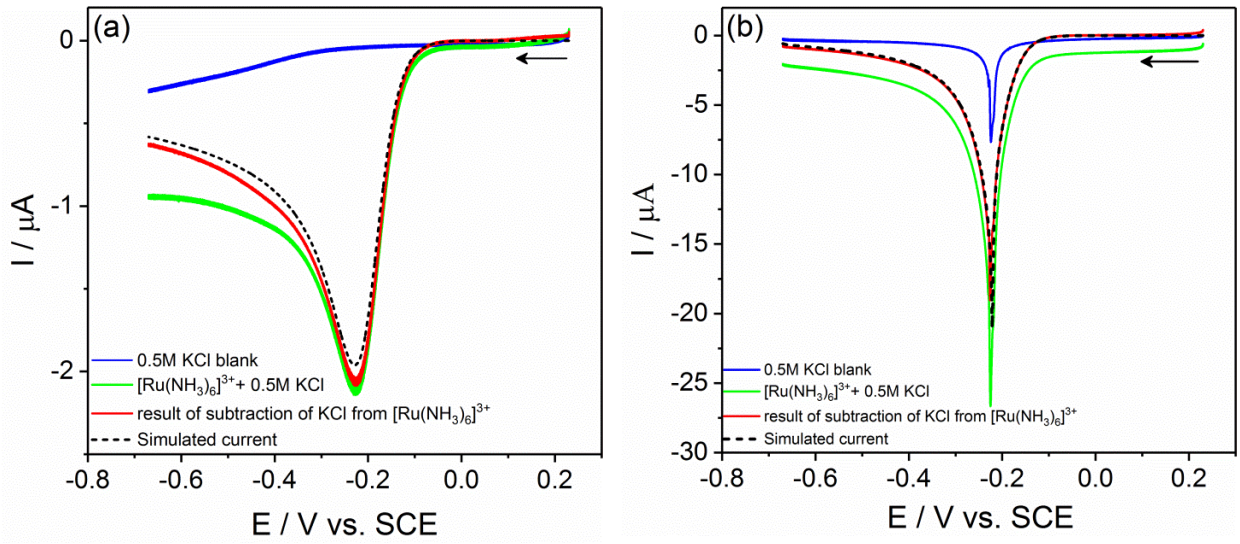

Fig. 2. Voltammograms obtained using (a) linear and (b) circular potential waveforms at a GC electrode in blank 0.50 M KCl solution (blue curves, capacitive currents) and in 0.265 mM $[Ru(NH_3)_6]Cl_3$/0.50 M KCl solution (green curves, faradaic + capacitive currents) at an average scan rate of 0.025 V s^{-1}. The experimental faradaic-only currents (red solid curves) are obtained by subtraction of the blue curve from the green curve and base line correction. The faradaic currents obtained from the simulations are displayed as black dashed lines. The arrows show the direction of potential sweep.

The voltammograms obtained from the semi-circular potential wave are different from those obtained using the conventional linear potential wave: the semi-circular wave results in a significantly larger (~ 10 times) peak current at −0.22 V than that obtained from the linear wave for the same potential window, and the current declines at other potentials of the voltammogram, see Fig. 2b. This noticeably high current response is due to the fact that the semi-circular potential wave generates a dramatically elevated scan rate at the midpoint of the applied potential window and slower scan rates everywhere else, and consequently when this increased scan rate occurs at and near the formal potential of $Ru^{3+/2+}$, a greater flux of Ru^{3+} to the electrode surface is achieved and thus a remarkable amplification of the peak current is observed, in agreement with the previous theoretical treatment of the method [19]. This method is therefore beneficial in electroanalysis because it possibly lowers the limit of detection of the species of interest by greatly amplifying the current response of such species, in particular when this species is present in a mixture with another species of similar formal potential.

The corresponding simulated currents (black dashed graphs) are displayed in Fig. 2. Diffusion coefficients *D* of 5.5×10^{-10} and 8.4×10^{-10} m^2 s^{-1} for Ruhex in 0.5 M and 0.1 M KCl, respectively, were used in the simulation [23]. The measured faradaic currents are in good agreement with the simulated currents.

4.2. Scan rate dependency of the voltammograms

Fig. 3 shows the voltammograms obtained at various scan rates between 0.01 and 1.6 V s^{-1} at the same GC electrode in 0.265 mM $[Ru(NH_3)_6]Cl_3$/0.50 M KCl solution. The potential was swept from 0.3 V to −0.6 V with E_{centre}= −0.15 V, which is 50 mV more positive to the formal potential (−0.200 V). For the semi-circular potential wave the duration of a single sweep was set in a way that the average scan rate is the same as that in the corresponding linear sweep voltammogram. In contrast to the linear sweep voltammogram which features a single peak, the semi-circle wave voltammogram shows two distinct peaks. First, a sharp peak on the right which coincides with the potential at which the scan rate reaches its maximum. The origin of this peak can be understood from the thermodynamics of the electrode reaction: The investigated redox system reacts reversibly and a thermodynamic equilibrium prevails at all time at the interface. Changes in the electrode potential result in instantaneous changes in the analyte concentration at the surface and simultaneously in a charge transfer at the electrode. In the here-investigated case, the current at a given position in the voltammogram increases with the scan rate and, consequently, the current reaches a peak at the maximum scan rate. Second, we observe a broader peak at ca. −0.20 V succeeding the sharp peak at ca. −0.15 V. This second peak arises from the interplay between changes in the analyte concentration at the surface induced from the altered electrode potential and the diffusive mass transport of analyte towards the surface, similar to the peak seen in linear voltammetry. In addition, in the semi-circular voltammograms, the peak position for both reduction peaks is shifted to more negative potentials with increasing the scan rate which could partially be due to an ohmic drop and partially due to bandwidth limitations in the application of the electrode potential. The sharp and broad peak currents of the semi-circular voltammograms are individually plotted. As shown in the inset in Fig. 3, independent of the applied potential waveform, a linear relationship is obtained between the measured faradaic current and the square root of the scan rate. For the linear sweep voltammetry of the reversible one-electron reduction of Ru^{3+}, such linearity is predicted by Randles-Ševčík equation [25] and is used to determine the diffusion coefficient of Ru^{3+} in 0.5M KCl. A value of D = (5.9 ± 0.4) x 10^{-10} m^2 s^{-1} is obtained, which is in good agreement with a formerly reported value of D = 5.5 x 10^{-10} m^2 s^{-1} [23]. With this high electrolytic support, the peak-to-peak separation is 59 ± 1 mV, as predicted for a reversible one-electron transfer process.

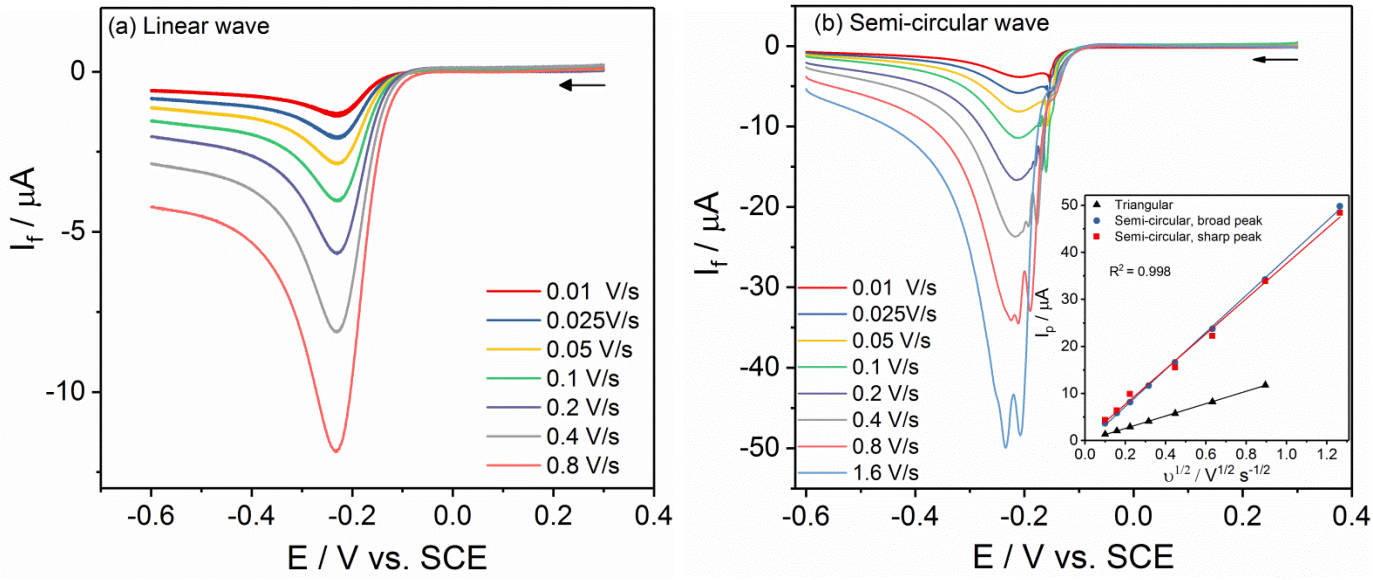

Fig. 3. Voltammograms obtained at different scan rates using (a) linear and (b) semi-circular waves in 0.265 mM $[Ru(NH_3)_6]Cl_3$/0.50 M KCl solution at 298 K. The inset of (b) is a plot of the resulting cathodic peak currents against the square root of the scan rate extracted from the corresponding data in the range of 0.01 to 1.6 V s^{-1}. Linear regressions are also shown. The experimental voltammograms are plotted after blank subtraction and baseline correction.

For semi-circular sweep voltammetry, using D = 5.5 x 10^{-10} m^2 s^{-1} [23], the linear regression of the peak currents reveals a pre-factor of 1.39 ± 0.02 and 1.32 ± 0.02 in Randles-Ševčík equation for the broad and the sharp peaks, respectively; the error bars of the pre-factors are based on the standard error of the slope. Notably, for the voltammograms of semi-circular waveforms, the pre-factor in the Randles-Ševčík equation is three times higher than that obtained from the linear wave, as can be expected from the nature of the semi-circular wave, see Fig. 1. We though note that the peak heights are limited by the accuracy and resolution at which we can apply potential waves and measure faradaic currents, particularly at fast scan rates.

4.3. Analysis of the semi-circular potential scans at shifted potential windows

In this and the following section, we first confirm the E_f^o of Ruhex from triangular voltage scan voltammograms, second use the value for the simulation of the semi-circular voltammograms, third compare the results of the simulation with the corresponding experimental result for the semi-circle wave to validate our theoretical model, and fourth validate the used E_f^o value.

The influence of shifting the potential window on the voltammetric response of both triangular and semi-circular potential waves is investigated first. Fig. 4 depicts the voltammograms obtained using triangular potential wave voltammetry in 0.265 mM $[Ru(NH_3)_6]Cl_3$/0.50 M KCl solution at 0.025 V s^{-1} and different potential windows. It is clear from direct observation that the voltammetric response

obtained is insensitive to the applied potential windows (i.e. different E_{centre} values): The triangular potential wave produces nearly identical voltammograms with single peaks at the same positions and magnitudes independent of the applied potential window. The formal potential is obtained from the midpoint between the reduction and oxidation peak potentials in the triangular voltammograms and a value of −200 ± 2 mV is obtained.

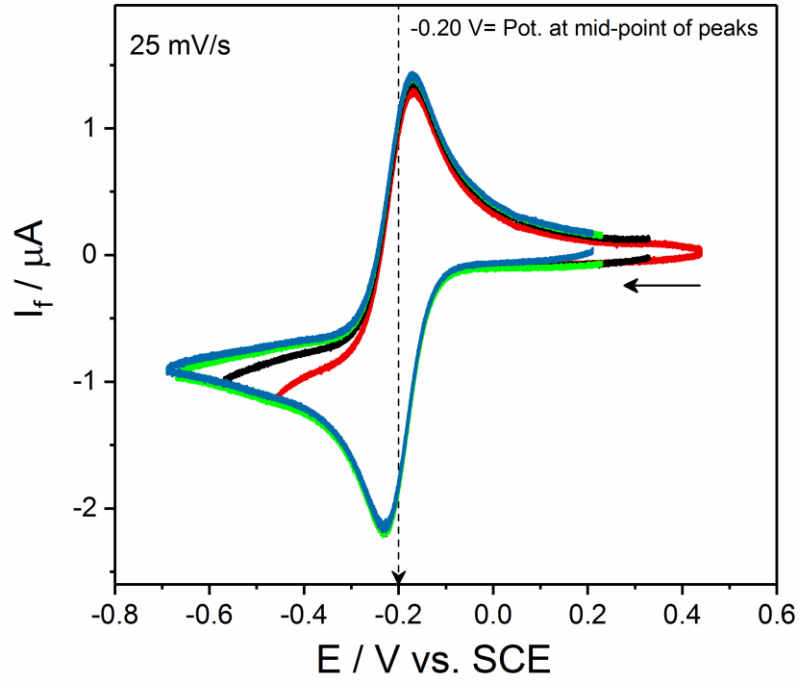

Fig. 4. Capacitance current-corrected voltammograms obtained at a GC electrode with the triangular potential waveform at different E_{centre} values at 0.025 V s^{-1} in 0.265 mM $[Ru(NH_3)_6]Cl_3$/0.50 M KCl solution at 298 K. The curves display the currents before baseline correction. The dashed arrow indicates the midpoint potential between the reduction and oxidation peak potentials.

The semi-circular potential wave was applied at different potential windows by changing the E_{centre} value for each sweep from −0.01 to −0.60 V in short intervals in the vicinity of the reduction peak. The voltammograms were recorded in 0.265 mM $[Ru(NH_3)_6]Cl_3$/0.50 M KCl solution at 298 K at the same GC working electrode. An average scan rate of 0.025 V s^{-1} was employed, which was achieved by setting the duration of each sweep to 36 s, as demonstrated in Fig. 1. Fig. 5 shows examples of the resulting experimental and corresponding simulated (using a formal potential of −200 mV) voltammograms of the semi-circle potential waveform at different potential windows. The used E_{centre} values are displayed in each graph.

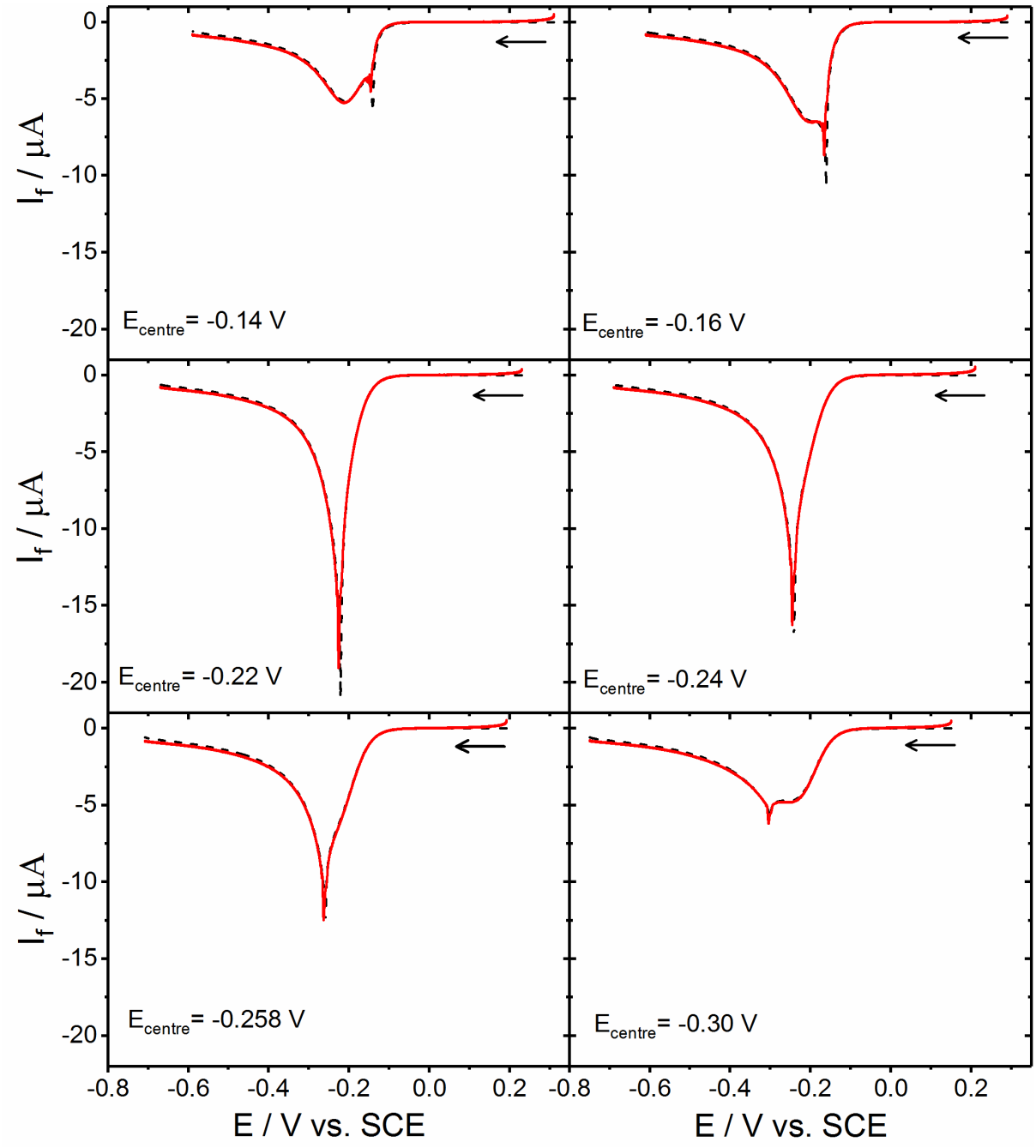

Fig. 5. Capacitance current- and base line-corrected voltammograms obtained from experiment (solid red curves) and simulation (dashed black curves) at a GC electrode using the semi-circular potential waveform at different E_{centre} values in 0.265 mM $[Ru(NH_3)_6]Cl_3$/0.50 M KCl solution at an average scan rate of 0.025 V s^{-1}.

In contrast to the linear wave voltammetry, the voltammetric behaviour obtained from the semi-circular potential wave is dependent on the applied E_{centre} value. In all semi-circular potential wave voltammograms, the current is largely amplified especially at the potential where the fastest scan rate occurs, generating a sharp peak at this potential. At certain E_{centre} values, two distinct peaks are observed: a slightly amplified broad reduction peak at potentials far from the set E_{centre} value and a

sharp peak at the fastest scan rate; the potential at which the sharp peak is observed is close to the applied E_{centre} value. It is also noteworthy to mention that in the blank solution the capacitive current shows a sharp peak with similar height at different potential windows, see Fig. S1.

Again, the emergence of a sharp peak in each voltammogram can be explained from the nature of the semi-circular wave function (Eq. 5) and its wave shape (Fig. 1): at the midpoint of the potential window, a steep slope is observed, which means a temporary fast scan rate (i.e. fast electron transfer kinetics), causing a significant rise in current, while relatively slower scan rates are applied everywhere else and the current decreases rapidly. The extent of the amplification of the peak current depends largely on the applied E_{centre} value as shown in Fig. 5: At E_{centre} values, for example at −0.14, −0.16 and −0.30 V, the fastest applied scan rate occurs at potentials far from the formal potential of $Ru^{3+/2+}$, and the peak current is low, but as the E_{centre} value approaches the formal potential the peak current increases dramatically (see curves at E_{centre} of −0.22 and −0.24 V), and it reaches a maximum at E_{centre} value where the fastest scan rate occurs few millivolts more negative than the formal potential of the species. An analysis of all measured voltammograms and their absolute peak heights is presented below and the exact potential, at which a maximum in the peak current is observed, is discussed.

From the above results, it can be seen that the peak current obtained using semi-circular potential wave is greatly amplified by a factor of ~10 when the fastest scan rate is applied in the close vicinity of the formal potential, while a much shorter sharp peak is seen when the fastest scan rate is applied at potentials far from the formal potential.

4.4. Determination of the formal potential of the redox couple $Ru[(NH_3)_6]^{3+/2+}$ using semi-circular voltammetry

Our previous work [19] showed how to sensitively determine the formal potential of a redox couple from a series of semi-circular voltammograms recorded at different E_{centre} values. Experimental voltammograms are herein first analysed to determine the E_{centre} value at which the maximum in peak currents occurs. This value is then compared with simulation results that relate the position of this peak in terms of E_{centre} to the formal potential. One advantage of our proposed method is that the determination of the formal potential is based only on the forward scan in contrast to the conventional CV, in which the peak-to-peak separation is used. This however relies on the backward peak for analysis which may not always be available. Another advantage is that the current response of this method is significantly higher than that of the conventional CV, and thus may reduce the limit of detection of the chemical species.

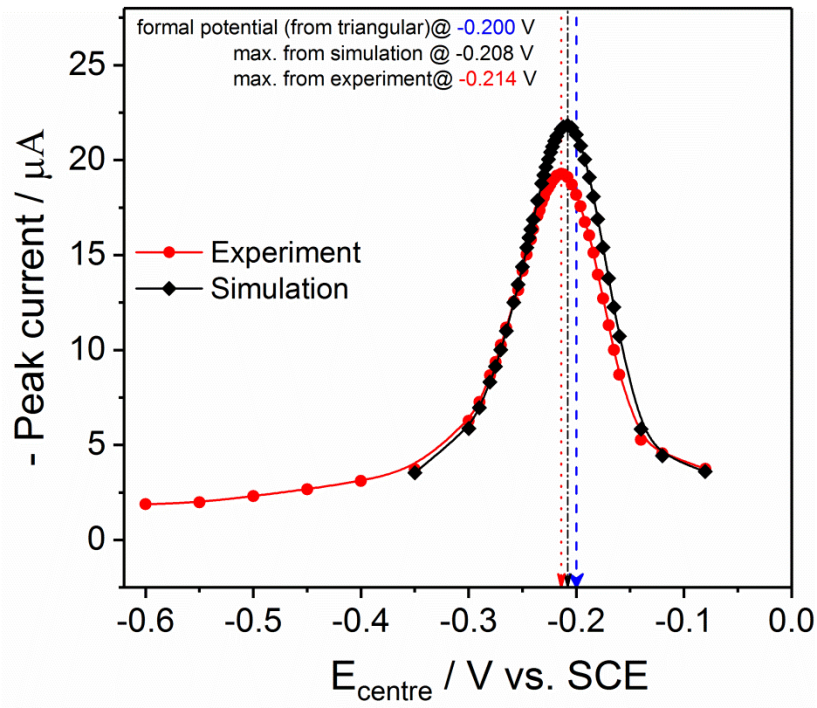

Fig. 6. Plot of the maximum peak currents for different E_{centre} values using the semi-circular potential wave. Data was obtained for 0.265 mM $[Ru(NH_3)_6]Cl_3$/0.50 M KCl at 0.025 V s^{-1} from the corresponding experimental (corrected for the capacitive current and the baseline, red spheres) and simulated (black diamonds) voltammograms. The formal potential estimated from the prior triangular voltammetry is indicated by the dashed blue line, while the simulated potential of the maximum peak current calculated using the E^o_f from the triangular wave voltammetry is indicated by the dash-dotted black line and from semi-circle experiment by the dotted red line.

Fig. 6 depicts the absolute maximum peak currents (red spheres) obtained experimentally at a scan rate of 0.025 V s^{-1} plotted against the corresponding E_{centre} value after the correction for capacitive currents and the base-line offset. We further plot the corresponding simulated peak currents (black diamonds) alongside the formal potential of −200 ± 2 mV as determined from Fig. 2 and 4 and on which basis data is simulated. In addition, we include the two peak positions, E^{max}_{centre}, in terms of E_{centre} as found experimentally and via the simulation at −214 ± 2 mV and −208 ± 2 mV, respectively. Errors indicate the resolution of the experimental and simulated data in terms of E_{centre}.

Fig. 6 shows good agreement between experiment and simulation, except of a different absolute magnitude of the simulated peak currents which, on the one hand, is due to the infinite current response expected at an infinite scan rate and bandwidth limitations of the potentiostat on the other. The combination of simulated and experimental data further allows the determination of the formal potential: The simulation reveals that, under the chosen experimental conditions, the peak in the plot of the absolute maximum currents as a function of E_{centre}, E^{max}_{centre}, is offset from the formal

potential by the theoretically predicted negative potential shift of $E_{centre}^{max} - E_f^o$ = −8 ± 1 mV. This finding can be exploited to, entirely independently from the prior measurements of the formal potential, determine the formal potential of the Ru^{3+}/Ru^{2+} couple experimentally from the semi-circular wave voltammetry: By simply calculating $E_f^o = (E_{centre}^{max} + 8)$ ± 1 mV, we determine the formal potential of −206 ± 2 mV from the semi-circular voltammetry. This value is in good agreement with the value determined from triangular voltammetry (−200 ± 2 mV), and the slight deviation of 6 ± 2 mV from simulation is attributed to bandwidth limitations of the digital-to-analogue converter which controls the electrode potential and an Ohmic drop at fast scan rates.

This above shows the experimental validation of the new semi-circular potential wave voltammetry and the use of this new method to measure the formal potential of $Ru^{3+/2+}$ redox couple.

5. Conclusions

We investigated voltammetry with a semi-circular potential waveform and experimentally verified our theoretical predictions using the reversible $[Ru(NH_3)_6]^{3+/2+}$ redox couple at a macroelectrode. Contrary to the classical linear potential wave, the semi-circular waveform has the characteristic feature that at the mid-point of the scanned potential window, a fast scan rate is obtained while relatively slower scan rates are found everywhere else. When the fastest scan rate appears within the close vicinity of the formal potential of $Ru^{3+/2+}$, a maximum in the absolute peak current is observed. In particular, experiments with a variable potential window relative to the formal potential show the presence of two peaks in the voltammograms for scans offset from being centred on E_f^o. The adjustment of the relative potential of the window allows the determination of the E_f^o value making use of the near infinite current expected for scans centred at E_f^o.

Acknowledgements

H. M. Amin gratefully acknowledges DFG for funding (No. AB 702/1-1). This work is partially funded from the European Research Council under the European Union's Seventh Framework Programme (FP/2007-2013)/ERC Grant Agreement No. 320403. The authors thank Dr. Christopher Batchelor-McAuley for writing the software.

Appendix A. Supplementary Information

Supplementary data to this article can be found online.

References

[1] A.J. Bard, L.R. Faulkner, Electrochemical Methods: Fundamentals and Applications, Wiley, 2001.
[2] R.G. Compton, C.E. Banks, Understanding Voltammetry, 2nd ed., Imperial College Press, 2011.
[3] F. Marken, A. Neudeck, A.M. Bond, Cyclic Voltammetry, in: F. Scholz (Ed.) Electroanalytical Methods: Guide to Experiments and Applications, Springer Berlin Heidelberg, Berlin, Heidelberg, 2002, pp. 51-97.
[4] Y. Uchida, E. Kätelhön, R.G. Compton, Cyclic voltammetry with non-triangular waveforms: Electrochemically irreversible and quasi-reversible systems, J. Electroanal. Chem., 810 (2018) 135-144.
[5] H.M.A. Amin, Y. Uchida, C. Batchelor-McAuley, E. Kätelhön, R.G. Compton, Non-triangular potential sweep cyclic voltammetry of reversible electron transfer: Experiment meets theory, J. Electroanal. Chem., 815 (2018) 24-29.
[6] Y. Uchida, E. Kätelhön, R.G. Compton, Cyclic voltammetry with non-triangular waveforms: Electrochemically reversible systems, J. Electroanal. Chem., 801 (2017) 381-387.
[7] R.S. Nicholson, I. Shain, Theory of Stationary Electrode Polarography. Single Scan and Cyclic Methods Applied to Reversible, Irreversible, and Kinetic Systems, Anal. Chem., 36 (1964) 706-723.
[8] R. Guidelli, R.G. Compton, J.M. Feliu, E. Gileadi, J. Lipkowski, W. Schmickler, S. Trasatti, Definition of the transfer coefficient in electrochemistry (IUPAC Recommendations 2014), Pure Appl. Chem., 86 (2014) 259-262.
[9] R. Guidelli, R.G. Compton, J.M. Feliu, E. Gileadi, J. Lipkowski, W. Schmickler, S. Trasatti, Defining the transfer coefficient in electrochemistry: An assessment (IUPAC Technical Report), Pure Appl. Chem., 86 (2014) 245-258.
[10] A.M. Bond, D. Elton, S.-X. Guo, G.F. Kennedy, E. Mashkina, A.N. Simonov, J. Zhang, An integrated instrumental and theoretical approach to quantitative electrode kinetic studies based on large amplitude Fourier transformed a.c. voltammetry: A mini review, Electrochem. Commun., 57 (2015) 78-83.
[11] E. Laviron, The use of linear potential sweep voltammetry and of a.c. voltammetry for the study of the surface electrochemical reaction of strongly adsorbed systems and of redox modified electrodes, J. Electroanal. Chem. Interfacial Electrochem., 100 (1979) 263-270.
[12] C. Amatore, E. Maisonhaute, B. Schöllhorn, Molecular electrochemistry pushed to its limits: from nanosecond kinetics to the dynamic study of nanometric objects, Actualite Chimique, (2008) 69-74.
[13] C. Amatore, E. Maisonhaute, When voltammetry reaches nanoseconds, Anal. Chem., 77 (2005) 303 A-311 A.
[14] P. Fortgang, C. Amatore, E. Maisonhaute, B. Schöllhorn, Microchip for ultrafast voltammetry, Electrochem. Commun., 12 (2010) 897-900.
[15] X.S. Zhou, B.W. Mao, C. Amatore, R.G. Compton, J.L. Marignier, M. Mostafavi, J.F. Nierengarten, E. Maisonhaute, Transient electrochemistry: beyond simply temporal resolution, Chem. Commun., 52 (2016) 251-263.
[16] A. Molina, J. Gonzalez, Pulse Voltammetry in Physical Electrochemistry and Electroanalysis. Theory and Applications, Springer International Publishing, Heidelberg, Germany, 2016.
[17] F. Scholz, Voltammetric techniques of analysis: the essentials, ChemTexts, 1 (2015) 17.
[18] F. Scholz, Electroanalytical Methods. Guide to experiments and applications, 2nd ed., Springer, Berlin, 2010.
[19] Y. Uchida, E. Kätelhön, R.G. Compton, Linear sweep voltammetry with non-triangular waveforms: New opportunities in electroanalysis, J. Electroanal. Chem., 818 (2018) 140-148.
[20] Y. Uchida, E. Kätelhön, R.G. Compton, Linear sweep voltammetry with non-triangular waveforms at a microdisc electrode, J. Electroanal. Chem., 823 (2018) 465-473.
[21] C. Batchelor-McAuley, J. Ellison, K. Tschulik, P.L. Hurst, R. Boldt, R.G. Compton, In situ nanoparticle sizing with zeptomole sensitivity, Analyst, 140 (2015) 5048-5054.

[22] E.J.F. Dickinson, J.G. Limon-Petersen, N.V. Rees, R.G. Compton, How Much Supporting Electrolyte Is Required to Make a Cyclic Voltammetry Experiment Quantitatively “Diffusional”? A Theoretical and Experimental Investigation, J. Phys. Chem. C, 113 (2009) 11157-11171.
[23] Y. Wang, J.G. Limon-Petersen, R.G. Compton, Measurement of the diffusion coefficients of $[Ru(NH_3)_6]^{3+}$ and $[Ru(NH_3)_6]^{2+}$ in aqueous solution using microelectrode double potential step chronoamperometry, J. Electroanal. Chem., 652 (2011) 13-17.
[24] M.C. Henstridge, E. Laborda, E.J.F. Dickinson, R.G. Compton, Redox systems obeying Marcus–Hush–Chidsey electrode kinetics do not obey the Randles–Ševčík equation for linear sweep voltammetry, J. Electroanal. Chem., 664 (2012) 73-79.
[25] J.E.B. Randles, A cathode ray polarograph. Part II. - The current-voltage curves, Transactions of the Faraday Society, 44 (1948) 327-338.